Journal of Materials Chemistry A

RSC Publishing

PAPER

View Article Online
View Journal | View Issue

Cite this: *J. Mater. Chem. A*, 2013, **1**, 5333

Synthesis of a novel and stable g-C_3N_4–Ag_3PO_4 hybrid nanocomposite photocatalyst and study of the photocatalytic activity under visible light irradiation†

Santosh Kumar,[a] T. Surendar,[a] Arabinda Baruah[b] and Vishnu Shanker*[a]

Received 13th January 2013
Accepted 26th February 2013

DOI: 10.1039/c3ta00186e

www.rsc.org/MaterialsA

A facile and reproducible template free *in situ* precipitation method has been developed for the synthesis of Ag_3PO_4 nanoparticles on the surface of a g-C_3N_4 photocatalyst at room temperature. The g-C_3N_4–Ag_3PO_4 organic–inorganic hybrid nanocomposite photocatalysts were characterized by various techniques. TEM results show the *in situ* growth of finely distributed Ag_3PO_4 nanoparticles on the surface of the g-C_3N_4 sheet. The optimum photocatalytic activity of g-C_3N_4–Ag_3PO_4 at 25 wt% of g-C_3N_4 under visible light is almost 5 and 3.5 times higher than pure g-C_3N_4 and Ag_3PO_4 respectively. More attractively, the stability of Ag_3PO_4 was improved due to the *in situ* deposition of Ag_3PO_4 nanoparticles on the surface of the g-C_3N_4 sheet. The improved performance of the g-C_3N_4–Ag_3PO_4 hybrid nanocomposite photocatalysts under visible light irradiation was induced by a synergistic effect, including high charge separation efficiency of the photoinduced electron–hole pair, the smaller particle size, relatively high surface area and the energy band structure. Interestingly, the heterostructured g-C_3N_4–Ag_3PO_4 nanocomposite significantly reduces the use of the noble metal silver, thereby effectively reducing the cost of the Ag_3PO_4 based photocatalyst.

1 Introduction

Semiconductor photocatalysis is an efficient technology for producing environmentally clean energy, in which one can use the sunlight as an energy source and it offers the possibility of accomplishing energy cycles without pollution of the environment and additional heating of the earth.[1,2] Unfortunately, most widely employed semiconductor photocatalysts are only active under UV-light irradiation, but photocatalysis using solar light could be highly economical compared to the process using an artificial UV-light source.[3,4] Therefore, development of efficient visible light driven photocatalysts is today's demand.

A few visible light photocatalysts, such as Ag-based photocatalysts, nanocomposite photocatalysts and g-C_3N_4 photocatalysts have attracted much attention for the photodegradation of organic pollutants and water splitting for environmentally clean energy in recent years.[5–12] However, a Ag_3PO_4 semiconductor has been reported as an active visible light driven photocatalyst for organic pollutants and hydrogen evolution from water splitting.[13,14] The photocatalytic performance of Ag_3PO_4 is significantly higher than that of currently known visible light photocatalysts, such as g-C_3N_4, N-doped TiO_2 and $BiVO_4$.[15–17] Unfortunately, this Ag_3PO_4 visible light photocatalyst is photochemicaly unstable, since silver salts are well known to decompose on light irradiation.[18] In addition to this stability, silver usage and the particle size of the Ag_3PO_4 photocatalyst remains relatively large, hindering its performance in photocatalytic processes for large scale applications. Therefore, a challenging task associated with this visible light photocatalyst is the synthesis of stable nano-sized Ag_3PO_4 particles with a high surface area. Thus, much attention has been employed to develop a simple and effective technology to reduce Ag consumption for a Ag_3PO_4 photocatalyst and to improve its stability and surface area for large scale applications.

On the other hand, the first metal free polymeric material, graphitic carbon nitride (g-C_3N_4) is one of the π-conjugated semiconductor materials possessing good photocatalytic activity for hydrogen production from water splitting and the photodegradation of organic pollutants under visible light irradiation.[19,20] The metal free g-C_3N_4 photocatalyst possesses a very high thermal and chemical stability, as well as electronic properties. However, the photocatalytic performance of g-C_3N_4 is still limited due to the high recombination rate of the photo-induced electron–hole pair. Therefore, making g-C_3N_4 a valuable material for visible light driven photocatalysts is important. Recently, several efforts have been made to improve the photocatalytic activity of g-C_3N_4 by employing different modifications, such as loading a co-catalyst onto the surface of g-C_3N_4, designing appropriate textural properties, doping and making composites with other semiconductor materials.[21–25] More recently Chengsi

[a]*Department of Chemistry, National Institute of Technology, Warangal-506004, A.P., India. E-mail: vishnu@nitw.ac.in; Fax: +91-870-2459547; Tel: +91-870-2462675*

[b]*Department of Chemistry, Indian Institute of Technology, Delhi, New Delhi-110016, India*

† Electronic supplementary information (ESI) available. See DOI: 10.1039/c3ta00186e

et al. reported a g-C_3N_4–$BiPO_4$ photocatalyst with a core–shell structure formed by a self assembly process and its application in the photocatalytic degradation of methylene blue (MB). The results showed that the photocatalytic activity of such a composite material was dramatically improved.[26]

In this work, we report a facile and reproducible template free *in situ* precipitation method for the synthesis of Ag_3PO_4 nanoparticles on the surface of a g-C_3N_4 photocatalyst at room temperature. The g-C_3N_4–Ag_3PO_4 organic–inorganic hybrid nanocomposite photocatalysts were characterised by XRD, TGA, FTIR, TEM, UV-Vis DRS and BET surface area analyser. The results demonstrated that after hybridization with g-C_3N_4, the stability of Ag_3PO_4 was enhanced under visible light irradiation and more attractively a dramatic photocatalytic activity under visible light irradiation was observed due to the introduction of g-C_3N_4 to Ag_3PO_4 which can effectively enhance the charge separation and photostability. The synergic effect between Ag_3PO_4 and g-C_3N_4, the possible mechanisms of photostability and enhancement of the photocatalytic activity *via* hybridization were also investigated. Therefore, the novel hetero-structured photocatalyst *i.e.* the combination of these two photocatalysts is of potential interest for overall water splitting *via* sunlight since g-C_3N_4 is a newly developed metal free hydrogen evolution photocatalyst, whereas the Ag_3PO_4 is also a newly developed water oxidation photocatalyst. Moreover, the silver weight percentage of the photocatalyst decreases extensively, thereby reducing the cost of Ag_3PO_4 based photocatalysts. It has also made the g-C_3N_4 as a valuable photocatalytic material for its potential applications in environmental protection. However, to the best of our knowledge there has been no report on the synthesis of a g-C_3N_4–Ag_3PO_4 organic–inorganic hybrid nanocomposite photocatalyst.

2 Experimental section

2.1 Materials

Melamine (Sigma-Aldrich, 99.0%), silver nitrate (Aldrich, 99.0%), liquid ammonia (Merck, 25.0%), sodium phosphate dodecahydrate (SISCO, 99.5%), ammonium oxalate (SISCO, 99.8%), terephthalic acid (Sigma-Aldrich, 98.0%) and methyl orange (Aldrich, 85.0%) were used as received. All other reagents used in this work were of an analytically pure grade and used without further purification.

2.2 Method

The preparation of the pure Ag_3PO_4 and g-C_3N_4–Ag_3PO_4 hybrid composites is shown by a schematic diagram (ESI, Fig. S1†). The g-C_3N_4 was prepared by direct heating of the melamine to 550 °C for 2 h in a N_2 atmosphere.[27] Pure Ag_3PO_4 was prepared by using an ion exchange method. 0.1 M aqueous solution of silver nitrate was added to a beaker and an aqueous solution of sodium phosphate dodecahydrate was added and stirred for 5 h at room temperature. The solution was centrifuged and the solid product washed (three times) with water and ethanol and then dried in an oven for 2 h at 100 °C. For the preparation of the g-C_3N_4–Ag_3PO_4 photocatalysts, an appropriate amount of g-C_3N_4 was ultrasonicated in 50 mL of water for 30 min. To this, 0.42 g of silver nitrate was added and stirred at room temperature for 1 h. Further, 50 mL of 0.1 M Na_3PO_4 was added and stirred for 5 h. The obtained solid product was centrifuged, washed and dried at 100 °C for 1 h. The g-C_3N_4–Ag_3PO_4 photocatalysts with different weight ratios of g-C_3N_4, particularly 25% and 40% were synthesized and named as CNAGPO25, and CNAGPO40 respectively. The pure g-C_3N_4 was named as CN and Ag_3PO_4 was named as AGPO.

2.3 Characterisation

Powder X-ray diffraction studies (PXRD) were carried out on a Bruker D_8 Advance diffractometer with a step size of 0.002° and a scan speed of 0.5 second per step in the 2θ range of 10° to 70°. TGA experiments were carried out on a PerkinElmer Pyris Diamond TGA/DTA system on well grounded samples in a flowing nitrogen atmosphere with a heating rate of 10 °C min^{-1}. FTIR spectra were recorded in transmission mode from 4000 to 400 cm^{-1} on a Nicolate Protégé 460 FTIR spectrometer using KBr discs. TEM was done on a JEOL, JSM-6700F instrument. UV-Vis diffuse reflectance spectra (UV-Vis DRS) were recorded on a Lambda/20 Instruments (UV-Vis NIR spectrophotometer), equipped with an integrating sphere and was used to record the diffuse reflectance spectra of the samples, and $BaSO_4$ was used as a reference. The nitrogen adsorption isotherm was carried out by using Quanta chrome NOVA 1200e. The photoluminescence (PL) spectra of the photocatalysts were recorded on a TSC Solutions F96PRO fluorescence spectrophotometer with an excitation wavelength of 365 nm.

2.4 Photocatalytic activity

Methyl orange (MO) was chosen as a model dye for the photocatalytic degradation experiments. The photocatalytic activity of the various samples (25 mg) were examined by monitoring the degradation of an aqueous suspension of MO (10 mg L^{-1}, 100 mL) in a beaker under a constant stirring condition at 250 rpm throughout the test at room temperature. The visible light source for the photo-irradiation was a solar simulator 300 W Xe lamp (Asahi Spectra Co. Ltd) with a super cold filter, which provides the visible light region ranging from 400 nm to 700 nm and a light intensity of 115 mW cm^{-2}. Prior to irradiation, photocatalysts were suspended in the solutions with constant stirring under dark conditions for 30 min to ensure that the surface of the catalyst was saturated with MO. During the photocatalysis processes, the samples were periodically withdrawn (sampling time of 5 min), centrifuged to separate the photocatalyst powder from the solution, and used for the absorbance measurement. The absorption spectra were recorded on a UV-Vis spectrophotometer. The photocatalytic activity of the composites was compared with the pure g-C_3N_4 and pure Ag_3PO_4 powders under the same experimental conditions.

2.5 Detection of reactive species

The reactive oxidative species detection process is similar to the photodegradation experimental process. Various scavengers were added into the methyl orange solution prior to addition of the photocatalyst. The dosages of these scavengers were used as

in the previous studies.[28,29] Further, photoluminescence (PL) spectra with terephthalic acid (TA) as a probe molecule were used to disclose the formation of ˙OH radicals on the surface of g-C_3N_4–Ag_3PO_4 under visible light irradiation. In a brief experimental procedure, CNAGPO25 (0.1 g) was dispersed in a 40 mL of the TA (5×10^{-4} mol L^{-1}) aqueous solution with NaOH (2×10^{-3} mol L^{-1}) at room temperature. The above suspension was subjected for the photocatalytic activity evaluation of the catalyst under visible light irradiation and the PL intensity was measured using a fluorescence spectrophotometer with an excitation wavelength of 365 nm.

3 Results and discussion

3.1 Catalyst characterization

The XRD patterns of the Ag_3PO_4, g-C_3N_4 and g-C_3N_4–Ag_3PO_4 photocatalysts are shown in Fig. 1. The results indicate that the diffraction peaks corresponding to the body-centred cubic phase of Ag_3PO_4 (JCPDS#060505) are retained for the g-C_3N_4–Ag_3PO_4 hybrid composites. There are crystalline g-C_3N_4 peaks in the g-C_3N_4–Ag_3PO_4 hybrid composite photocatalysts, the peak intensities increased with the increase in g-C_3N_4 loading.

TGA was carried out for the g-C_3N_4 and g-C_3N_4–Ag_3PO_4 samples. The amount of loaded g-C_3N_4 was confirmed by TG analysis. For pure g-C_3N_4, a weight loss occurring from 550 °C to 720 °C could be attributed to the burning of g-C_3N_4. This weight loss region could be seen in all g-C_3N_4–Ag_3PO_4 hybrid composites. The amount of g-C_3N_4 in the hybrid composite was calculated from the corresponding weight loss and is shown in Fig. 2. The g-C_3N_4 in the loaded compositions of 1 : 3 and 2 : 3 weight ratios of g-C_3N_4–Ag_3PO_4 was found to be 27 wt% and 42 wt% respectively. Therefore, the amount of g-C_3N_4 was nearly consistent to the dosage of g-C_3N_4 loaded.

The FTIR spectra of g-C_3N_4, Ag_3PO_4 and g-C_3N_4–Ag_3PO_4 photocatalysts are shown in Fig. 3. In the FTIR spectrum of g-C_3N_4, the broad bands around 3100 cm^{-1} are indicative of N–H stretching vibrations, the peaks at 1243 cm^{-1} and 1637 cm^{-1} correspond to the C–N and C=N stretching vibrations,

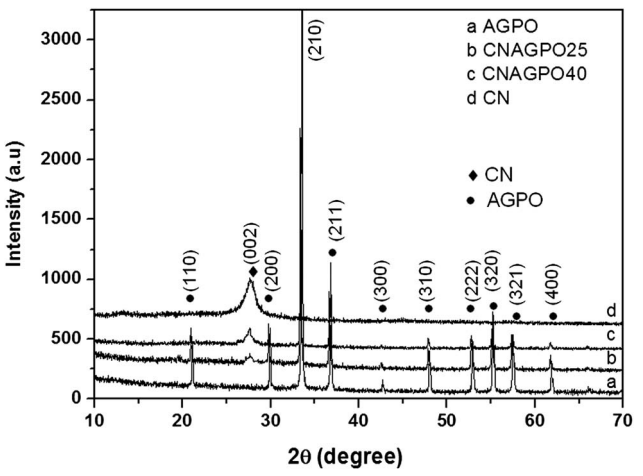

Fig. 1 XRD patterns of the as synthesized g-C_3N_4, Ag_3PO_4 and g-C_3N_4–Ag_3PO_4 photocatalysts.

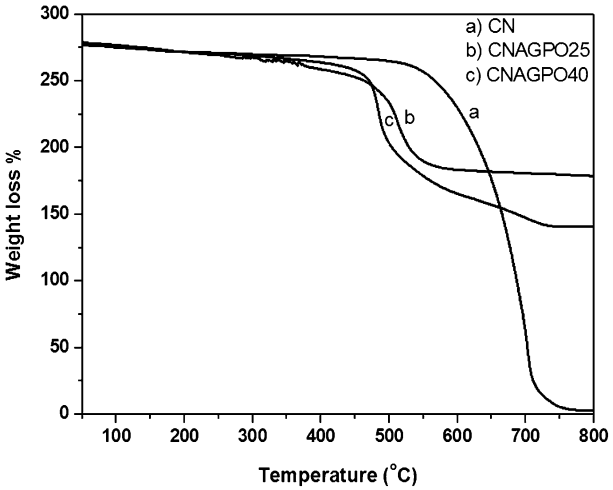

Fig. 2 TG curves of the as synthesized g-C_3N_4 and g-C_3N_4–Ag_3PO_4 photocatalysts.

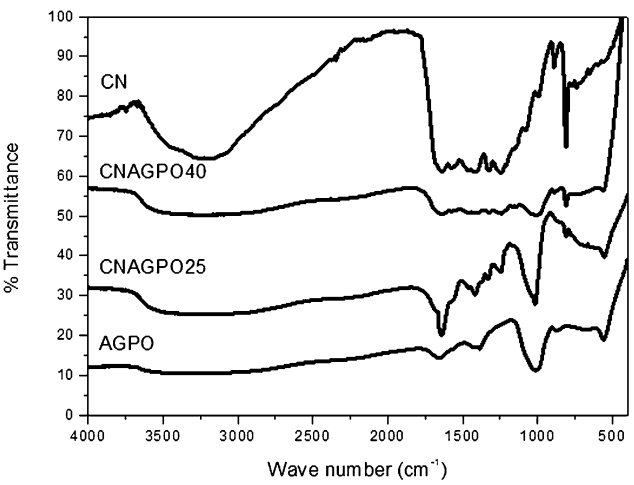

Fig. 3 FTIR of the as synthesized g-C_3N_4, Ag_3PO_4 and g-C_3N_4–Ag_3PO_4 photocatalysts.

respectively. The peak at 808 cm^{-1} is related to the s-triazine ring vibrations.[30–32] In the FTIR spectrum of Ag_3PO_4, the broad absorption peaks were around 3300–3600 cm^{-1} and 1658 cm^{-1} corresponding to OH stretching vibrations, and the peak at 1384 cm^{-1} is corresponding to the H–O–H bending band of the adsorbed H_2O molecules on the surface of the products. The two peaks at 1015 cm^{-1} and 560 cm^{-1} are corresponding to the P–O stretching vibrations of PO_4^{3-}.[33–35] All the characteristic peaks of g-C_3N_4 and Ag_3PO_4 were observed in the g-C_3N_4–Ag_3PO_4 hybrid composite photocatalysts.

UV-Vis diffuse reflectance measurements of g-C_3N_4, Ag_3PO_4 and g-C_3N_4–Ag_3PO_4 composites are shown in Fig. 4. In the g-C_3N_4–Ag_3PO_4 hybrid composite photocatalyst there is a small shift in the band edge positions to a higher wavelength as compared with pure g-C_3N_4 and pure Ag_3PO_4 suggesting that the recombination rate of the electron–hole pair was successfully reduced in the heterostructured g-C_3N_4–Ag_3PO_4 hybrid composite photocatalyst.

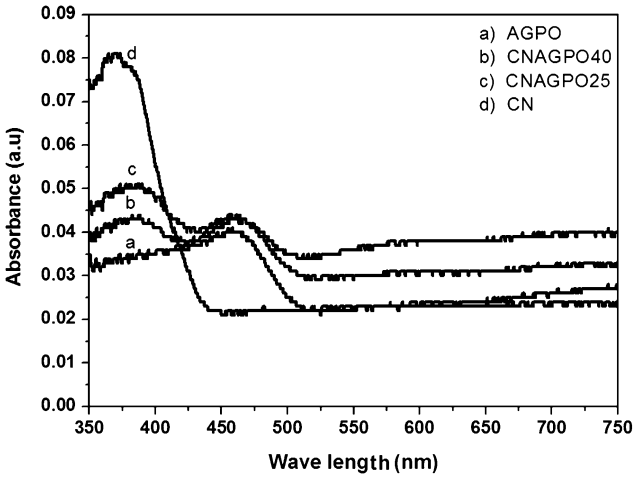

Fig. 4 UV-Vis DRS of the as synthesized g-C_3N_4, Ag_3PO_4 and g-C_3N_4–Ag_3PO_4 photocatalysts.

The morphology of all the as synthesised photocatalysts was investigated by TEM. Fig. 5 shows the TEM images of the pure g-C_3N_4 and Ag_3PO_4 samples. Fig. 5(a) and (b) show the pure g-C_3N_4 sample consists of submicrometer sheets with and Ag_3PO_4 particles ranging from 200–800 nm respectively. There is no distinctive morphological features appearing for the Ag_3PO_4 particles. Fig. 6 shows the TEM images of the composite photocatalyst. Fig. 6(a)–(d) illustrate the uniform deposition of Ag_3PO_4 nanoparticles on g-C_3N_4 sheet. The size of Ag_3PO_4 nanoparticles was found to be around 12 nm. TEM studies confirm that g-C_3N_4 sheet could serve as a support and surfactant to bound Ag_3PO_4 particles in this composite system. Our results clearly indicate that in composite samples, Ag_3PO_4 nanoparticles were uniformly distributed on g-C_3N_4 sheet, no apparent aggregation of the Ag_3PO_4 nanoparticles was discerned which leads to the formation of interfaces between Ag_3PO_4 and g-C_3N_4. The specific surface area and pore size distribution of g-C_3N_4–Ag_3PO_4 were investigated by nitrogen adsorption–desorption analysis (ESI, Fig. S2†). The specific surface areas of the as synthesized CNAGPO25 and CNAGPO40 were 11.24 $m^2\ g^{-1}$ and 12.38 $m^2\ g^{-1}$ respectively. The specific surface area of these composites is quite a bit higher than that of pure g-C_3N_4 (8 $m^2\ g^{-1}$), but it is much higher than that of pure Ag_3PO_4 (0.89 $m^2\ g^{-1}$).[12,15] This might be due to the Ag_3PO_4 nanoparticles being deposited on the g-C_3N_4 surface. A large specific surface area is useful for adsorption of organic compounds, and further enhances the efficiency of the photocatalytic process because the adsorption of organic compounds on the surface of the photocatalyst is the initial step of the photocatalytic oxidation of organic compounds. In addition to this, large surface area provides a higher number of reactive sites for the photocatalytic process. Therefore, uniformly distributed Ag_3PO_4 nanoparticles on g-C_3N_4 sheets with a high surface area can lead to a better interaction between g-C_3N_4 and Ag_3PO_4 improving the photocatalytic performance of hybrid composites under visible light irradiation.

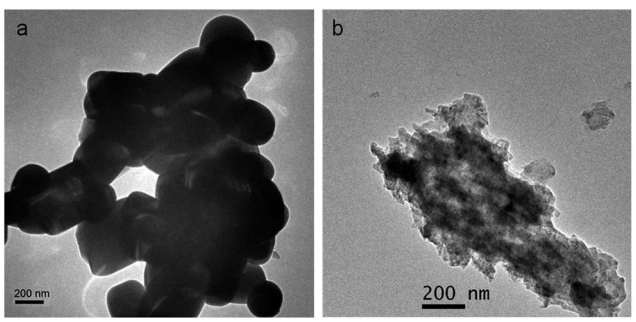

Fig. 5 TEM images of the as synthesized Ag_3PO_4 and g-C_3N_4 photocatalyst: (a) pure Ag_3PO_4, (b) pure g-C_3N_4.

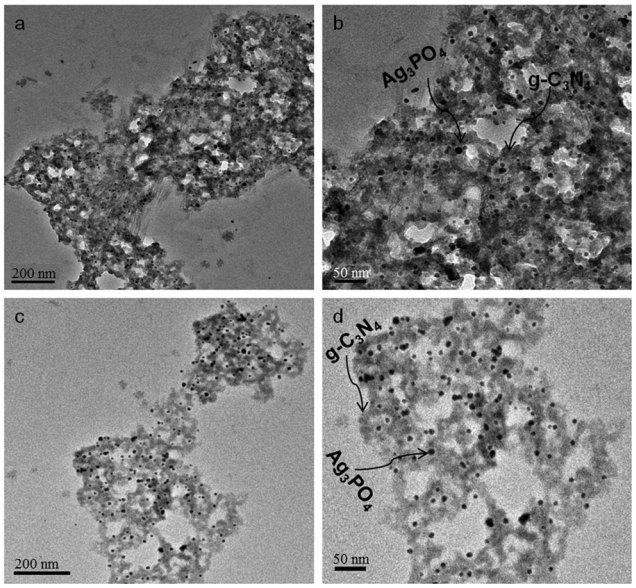

Fig. 6 TEM images of the as synthesized g-C_3N_4–Ag_3PO_4: (a) CNAGPO25, (b) CNAGPO25 (magnified), (c) CNAGPO40 and (d) CNAGPO40 (magnified).

3.2 *In situ* growth strategy

Direct growth is widely used to prepare different kinds of composite such as graphene based metal compounds such as graphene–metal oxide, and graphene–metal sulphides.[36,37] In the present work, we report an *in situ* growth strategy for the synthesis of a g-C_3N_4–Ag_3PO_4 organic–inorganic hybrid composite as shown in Fig. 7. The precursor for Ag_3PO_4 is silver nitrate. Silver salt is mixed with an ultrasonically dispersed g-C_3N_4 sheet which is synthesized by direct heating of the melamine at 550 °C for 2 h. The Ag^+ ions from the silver salt can be bound to the surface of the g-C_3N_4 due to chemical adsorption and these Ag^+ ions were converted into Ag_3PO_4 nanoparticles due to ion exchange, with the addition of sodium phosphate dodecahydrate as a precipitating agent, under constant stirring at room temperature. Thus, finely distributed uniform Ag_3PO_4 nanoparticles were successfully deposited on the surface of the g-C_3N_4 sheet. In the hybrid composite, the size of Ag_3PO_4 nanoparticles formed on g-C_3N_4 sheets were around 12 nm. The *in situ* growth strategy could avoid the particle agglomeration of Ag_3PO_4 on the g-C_3N_4 sheet, resulting in a uniform distribution of Ag_3PO_4 nanoparticles on the g-C_3N_4 surface. This *in situ* precipitation method for the synthesis of a g-C_3N_4–Ag_3PO_4

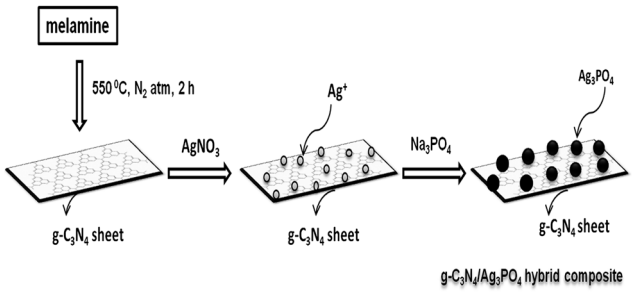

Fig. 7 Schematic representation for the *in situ* deposition of Ag_3PO_4 nanoparticles on g-C_3N_4 sheets.

hybrid composite photocatalyst can also be summarized as follows:

$$\text{g-}C_3N_4(s) + Ag^+(aq) \rightarrow \text{g-}C_3N_4\text{–}Ag^+(ad);\ pH = 7$$

$$\text{g-}C_3N_4\text{–}Ag^+(ad) + PO_4^{3-}(aq) \rightarrow \text{g-}C_3N_4\text{–}Ag_3PO_4;\ pH = 7$$

3.3 Photocatalytic performance

The photocatalytic activities of the as synthesized samples were evaluated *via* the photodegradation of MO under visible light irradiation, as shown in Fig. 8. The photolysis of MO was also studied for same duration under visible light irradiation in the absence of catalyst which indicates that MO is stable under visible light irradiation. The g-C_3N_4–Ag_3PO_4 photocatalysts showed much higher photocatalytic activities for the photodegradation of MO than pure g-C_3N_4 and Ag_3PO_4. Moreover, the photocatalytic activity of g-C_3N_4–Ag_3PO_4 photocatalyst with a 1 : 3 weight ratio was almost 5 times higher than that of pure g-C_3N_4 and 3.5 times higher than pure Ag_3PO_4. Our results clearly indicate that the g-C_3N_4–Ag_3PO_4 composite has better performance in the photodegradation of organic pollutant than the pure g-C_3N_4 and Ag_3PO_4 prepared under the same experimental conditions. However, when the g-C_3N_4 content increased from 25 wt% to 40 wt% there was a slight decrease in photocatalytic activity, but it was much higher compared to the photocatalytic activity of pure g-C_3N_4 and Ag_3PO_4. The much higher content of g-C_3N_4 in the composite may make an unsuitable ratio between g-C_3N_4 and Ag_3PO_4, thereby lowering the electron transfer efficiency of the photoinduced electrons on Ag_3PO_4 nanoparticles to g-C_3N_4 surfaces, thus the activity goes down with much higher loading in the composite photocatalyst under visible light irradiation. This result indicates that both g-C_3N_4 and Ag_3PO_4 play an important role in improving the photocatalytic activity, due to the significant synergistic effect between g-C_3N_4 and Ag_3PO_4 for the photodegradation of MO under visible light irradiation.

3.4 Photoluminescence

Enhanced photocatalytic activity was observed for the synthesized g-C_3N_4–Ag_3PO_4 hybrid composites, as shown in Fig. 8. This is because the Ag_3PO_4 and g-C_3N_4 have more closely contacted interfaces. This can be observed by the photoluminescence (PL) spectra, which are useful to explain the migration, transfer, and recombination processes of the photoinduced electron–hole pairs in the semiconductors.[38,39] Fig. 9 shows the PL spectra of Ag_3PO_4, g-C_3N_4 and g-C_3N_4–Ag_3PO_4 composites at room temperature. Obviously, the pure g-C_3N_4 and Ag_3PO_4 have a strong and wide peak around 450 nm and 520 nm respectively in the PL spectrum. However, in the case of the g-C_3N_4–Ag_3PO_4 hybrid nanocomposite, the photoinduced electron–hole pair can migrate easily between g-C_3N_4 and Ag_3PO_4 due to their matching band potentials and therefore, the recombination of electrons and holes is greatly hindered. This result shows that the g-C_3N_4–Ag_3PO_4 composite is useful to reduce the recombination rate of the photoinduced electron–hole pair and improve the corresponding photocatalytic activity. So, no photoluminescence can be observed. This result shows good agreement with the other p–n heterojunction semiconductors.[39] Thus, the hybrid composites with matched energy band positions could be promising photocatalysts for environmental applications.

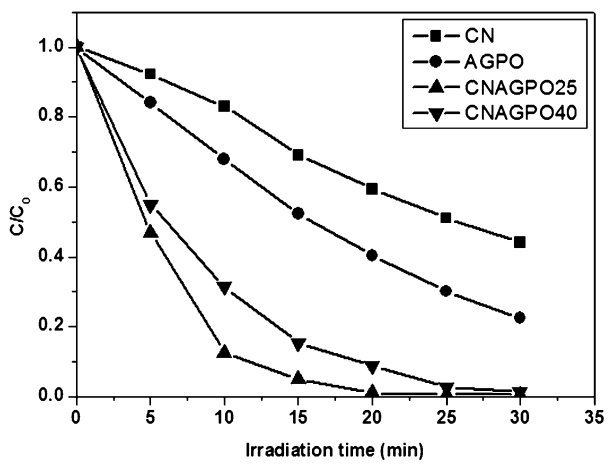

Fig. 8 Photocatalytic degradation of MO in aqueous solution over g-C_3N_4, Ag_3PO_4 and g-C_3N_4–Ag_3PO_4 photocatalysts.

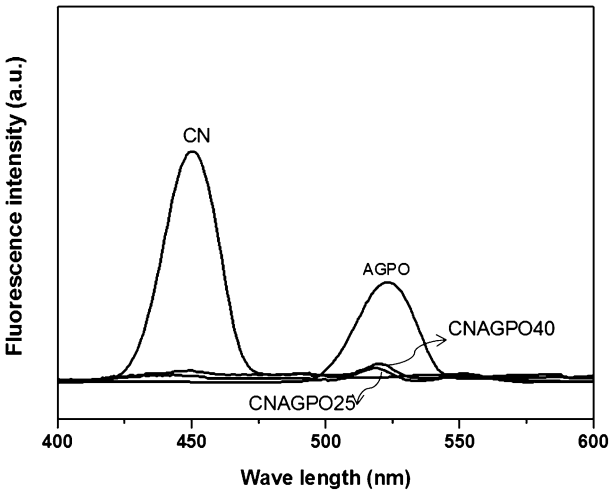

Fig. 9 Photoluminescence (PL) spectra of the as synthesized g-C_3N_4, Ag_3PO_4 and g-C_3N_4–Ag_3PO_4 photocatalysts at room temperature.

3.5 Reusability

The stability of a photocatalyst is also very important from point of view of its practical application. However, it is well know that the pure Ag_3PO_4 would photochemically decompose if no sacrificial reagent was involved in the process.[18] During the photocatalytic process, in the case of pure Ag_3PO_4, we also observed the yellow colour turned darker when the photocatalytic reaction was completed. This indicates the formation of Ag^0 species due to the reduction of Ag^+ from Ag_3PO_4 by photoinduced electrons as Ag_3PO_4 is unstable under photo irradiation, which may reduce the structural and photochemical stabilities.[40] More importantly, the g-C_3N_4–Ag_3PO_4 hybrid composite photocatalysts were found to be more stable than pure Ag_3PO_4 under similar conditions, as shown in Fig. 10. To study the stability of the g-C_3N_4–Ag_3PO_4 hybrid composite photocatalyst, the six successive photocatalytic experiments were carried out by adding used Ag_3PO_4 and g-C_3N_4–Ag_3PO_4 photocatalysts to fresh MO solutions with no change in the overall concentration of the catalyst (2–3 mg catalyst loss for each experimental run). The photocatalytic activity of g-C_3N_4–Ag_3PO_4 was retained at over 90% of its original activity after six successive experimental runs, which promotes the photocatalyst for its practical applications in environmental protection. The XRD studies were performed for Ag_3PO_4 and g-C_3N_4–Ag_3PO_4 after six successive experimental runs (ESI, Fig. S3†). For pure Ag_3PO_4, it is observed that a new peak corresponding to Ag^0 appeared together with the XRD peaks of Ag_3PO_4 after the six successive experimental runs, whereas no such peak was observed in the g-C_3N_4–Ag_3PO_4 hybrid composites. This indicates that the Ag_3PO_4 nanoparticles were tightly bound with the surface of the g-C_3N_4 sheet, which promotes the stability of the g-C_3N_4–Ag_3PO_4 composite photocatalysts due to the chemical adsorption between N–H groups or π-electrons in g-C_3N_4 and Ag^+ ions in Ag_3PO_4. Therefore, g-C_3N_4–Ag_3PO_4 composites can be used as high-performance and stable visible-light photocatalysts and their potential applications in environmental protection.

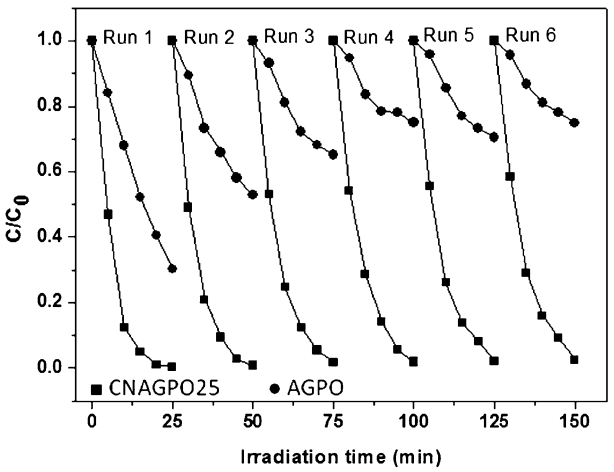

Fig. 10 Recyclability of the CNAGPO25 photocatalyst in six successive experiments for the photocatalytic degradation of MO in aqueous solution under visible light irradiation (no change in overall catalyst concentration for each run).

3.6 Mechanism for the improved photocatalytic activity and stability of the g-C_3N_4–Ag_3PO_4 composite

It is well known that an efficient charge separation, large surface area and high adsorption ability play an important role for the enhancement of photocatalytic activity.[5] The g-C_3N_4 has been shown to be an effective electron transporter and acceptor in the systems of g-C_3N_4–TiO_2, g-C_3N_4–ZnO and g-C_3N_4–$BiPO_4$. The g-C_3N_4 sheets could facilitate charge migration and reduce the recombination of electron–hole pairs of the g-C_3N_4 based photocatalysts.[9,26,41] Our results also clearly indicate that reinforced charge migration might be achieved in the as synthesized g-C_3N_4–Ag_3PO_4 hybrid composite. However, few reports have shown the partial reduction of Ag^+ ion into Ag metal, which could act as electron acceptors to make the photoexcited electrons migrate from Ag_3PO_4, and effectively protect Ag_3PO_4 from further photoreduction of the Ag^+ ion in Ag_3PO_4.[42,43]

On the basis of the above results, a proposed mechanism is discussed to explain that the enhanced photocatalytic activity and stability of the g-C_3N_4–Ag_3PO_4 photocatalysts is due to synergistic effects between the Ag_3PO_4 nanoparticles and the g-C_3N_4 sheet. First, the deposition of Ag_3PO_4 nanoparticles on the surface of the insoluble g-C_3N_4 sheet of Ag_3PO_4 can effectively protect Ag_3PO_4 from dissolution in aqueous solution due to chemical adsorption between g-C_3N_4 and Ag_3PO_4, thus the structural stability of g-C_3N_4–Ag_3PO_4 can be greatly enhanced during the photocatalytic reaction. Second, the high separation efficiency may be due to the energy level match between g-C_3N_4 and Ag_3PO_4. According to the previous reports, the redox potential of both conduction band (E_{CB} = −1.3 eV *vs.* NHE) and valence band (E_{VB} = +1.4 eV *vs.* NHE)[15] of g-C_3N_4 are more negative than those of the conduction band (E_{CB} = +0.45 eV *vs.* NHE) and valence band (E_{VB} = +2.9 eV *vs.* NHE)[18] of Ag_3PO_4. A scheme for the separation and transport of photogenerated electron–hole pairs at the g-C_3N_4–Ag_3PO_4 interface is shown in Fig. 11. Under the visible light irradiation a high-energy photon excites an electron from the valence band (VB) to the conduction band (CB) of Ag_3PO_4 and g-C_3N_4. The photoinduced electrons in g-C_3N_4 can move freely towards the surface of the Ag_3PO_4 while the holes can transfer to the VB of g-C_3N_4 conveniently and *vice versa*, since band edges of both g-C_3N_4 and Ag_3PO_4 lie in the visible region. Therefore, g-C_3N_4 can act as both an electron acceptor and donor. Hence the electrons can easily migrate to the surface of Ag_3PO_4 and the redundant electrons on Ag_3PO_4 can also be transferred to g-C_3N_4. As a result, the photogenerated electrons and holes are efficiently separated between Ag_3PO_4 and g-C_3N_4 thereby enhances the photocatalytic activity. Interestingly, the efficient electron migration from Ag_3PO_4 to g-C_3N_4 sheets also promotes the stability of the g-C_3N_4–Ag_3PO_4 composite by keeping electrons away from the Ag_3PO_4. This effective separation of photogenerated electron–hole pairs driven by band potentials between two semiconductors is also reported in other systems, such as g-C_3N_4–TaON.[44] Third, the g-C_3N_4 can act as an electron reservoir to trap electrons emitted from Ag_3PO_4 particles due to irradiation by visible light, thus protecting the electron–hole pair from recombination in the g-C_3N_4–Ag_3PO_4 hybrid composite photocatalysts. The electrons on g-C_3N_4 could also adsorb surface O_2 form various reactive oxygen species, thus

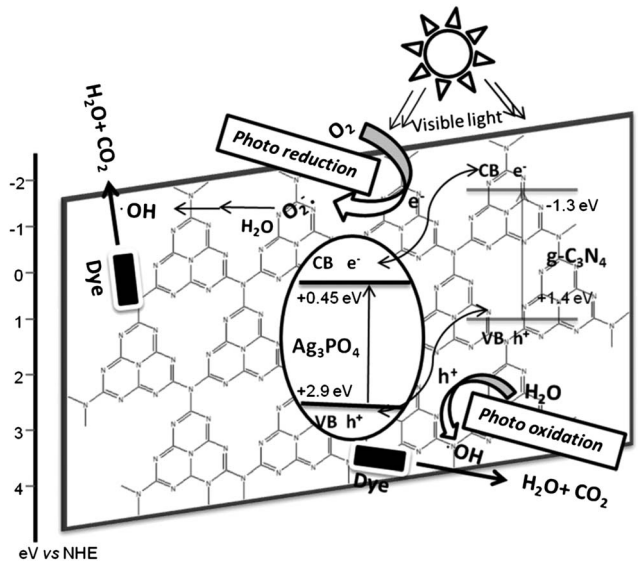

Fig. 11 Schematic diagram showing the process of the photocatalytic dye degradation over the g-C_3N_4–Ag_3PO_4 composite.

could assist the degradation of organic MO effectively. Meanwhile, the photogenerated holes on Ag_3PO_4 could also oxidize polluted dyes. Fourth, monodispersed uniform Ag_3PO_4 nanoparticles with high surface area from its bulk counterpart were successfully deposited on the surface of g-C_3N_4 sheet and could also account for the enhanced photocatalytic activity in the hybrid composite. Fifth, the high adsorption ability of g-C_3N_4 towards the organic pollutant since the high level of Ag^+ ion release in hybrid composite increase adsorption capability of g-C_3N_4 to the organic pollutant. These above aspects together contributed to the enhanced photocatalytic activity and improved stability of this novel g-C_3N_4–Ag_3PO_4 hybrid composite photocatalyst compared to pure Ag_3PO_4 particles.

3.7 Detection of reactive oxidative species

The dramatic photocatalytic activity of the as synthesized hybrid composite motivated us to further investigate the photocatalytic pathway of the degradation process. Generally, photoinduced reactive species including trapped holes, ·OH radicals, and $O_2^{\cdot-}$ are expected to be involved in the photocatalytic process. To examine the role of these reactive species, the effects of some radical scavengers and N_2 purging on the photodegradation of methyl orange were investigated to propose a reaction pathway. As the photoinduced electron–hole pair separated in the hybrid composite photocatalyst, the photoinduced holes could directly oxidize the adsorbed H_2O molecules to ·OH radicals on the surface of Ag_3PO_4 nanoparticles because the E_{VB} (Ag_3PO_4, +2.9 eV *vs.* NHE) is higher than $E_{(OH/H_2O)}$ (+2.68 eV *vs.* NHE). However, the E_{CB} (Ag_3PO_4, +0.45 eV *vs.* NHE) is also higher than $E_{(O_2/O_2^{\cdot-})}$ (+0.13 eV *vs.* NHE), which cannot produce $O_2^{\cdot-}$ radicals from dissolved O_2 by photoinduced electrons in Ag_3PO_4, but the $E_{(CB)}$ (g-C_3N_4, −1.3 eV *vs.* NHE) of g-C_3N_4 is lower than $E_{(O_2/O_2^{\cdot-})}$, so the $O_2^{\cdot-}$ radicals can still be produced in the g-C_3N_4–Ag_3PO_4 photocatalyst. As can be seen from Fig. 12a, when N_2 purging was conducted which acts as an $O_2^{\cdot-}$ radicals scavenger, no change was observed in the degradation of methyl orange compared with air-equilibrated conditions *i.e.* in the absence of scavenger, which confirms that the dissolved O_2 has no effect on the photodegradation process under visible light irradiation. A significant change was observed in the photocatalytic degradation of methyl orange by the addition methanol as the ·OH scavenger compared with no scavenger at the same conditions. However, the degradation rate was drastically inhibited by the addition of ammonium oxalate (AO) as a holes scavenger, indicating that the superoxide radicals are not the main active oxidative species of the g-C_3N_4–Ag_3PO_4 hybrid composite photocatalyst, but the holes and/or ·OH radicals can play an important role in the photodegradation of methyl orange under visible light irradiation. Further, it was confirmed by ·OH trapping PL spectra of CNAGPO25 with TA solution under visible light irradiation (Fig. 12b).

4 Conclusion

In summary, a novel and stable g-C_3N_4–Ag_3PO_4 organic–inorganic hybrid composite photocatalyst has been synthesized by a facile and reproducible template free *in situ* precipitation method at room temperature. More attractively, the dramatic visible light photocatalytic activity is generated due to the *in situ* deposition of monodispersed uniform Ag_3PO_4 nanoparticles on the surface of the g-C_3N_4 sheet. Furthermore, the heterostructure improved the stability of the Ag_3PO_4 nanoparticles on the surface of the g-C_3N_4 sheet. On the basis of our analysis, it is

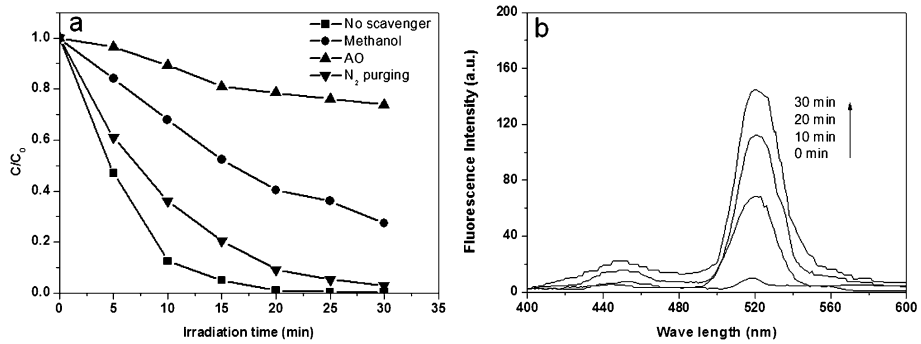

Fig. 12 (a) Effects of different scavengers on the degradation of methyl orange in the presence of CNAGPO25 catalyst under visible light irradiation, (b) ·OH trapping PL spectra of CNAGPO25 with TA solution under visible light irradiation.

assumed that the improved photocatalytic activity and stability of g-C_3N_4–Ag_3PO_4 hybrid composites under visible light irradiation might be a synergistic effect, including the high charge separation efficiency of photoinduced electron–hole pair, high structural stability, the smaller particle size, relatively high surface area and the energy band structure. The reactive oxidative species detection studies indicated that the photodegradation of methyl orange over the as synthesized g-C_3N_4–Ag_3PO_4 under visible light is mainly *via* holes and ·OH species. Therefore, the facile and reproducible template free *in situ* precipitation method is expected to be extended for depositing other nanoparticles on the surface of the g-C_3N_4 sheets.

Acknowledgements

The authors thank DST, Govt. of India for financial support (SR/FT/CS-096/2009). Santosh Kumar also thanks MHRD, Govt. of India for a fellowship. The corresponding author also thanks Prof. A. K. Ganguli, Indian Institute of Technology Delhi, for carrying out part of this work in his lab.

References

1 M. R. Hoffmann, S. T. Martin, W. Y. Choi and D. W. Bahnemann, *Chem. Rev.*, 1995, **95**, 69.
2 Y. T. Wey, A. S. Jason and A. Rose, *J. Phys. Chem. Lett.*, 2012, **3**, 629.
3 K. Anna, F. G. Marcos and C. Gerardo, *Chem. Rev.*, 2012, **112**, 1555.
4 K. Rajeshwara, M. E. Osugib, W. Chanmaneec, C. R. Chenthamarakshana, M. V. B. Zanonib, P. Kajitvichyanukuld and R. Krishnan-Ayera, *J. Photochem. Photobiol., C*, 2008, **9**, 171.
5 P. Wang, B. Huang, Y. Dai and M. H. Whangbo, *Phys. Chem. Chem. Phys.*, 2012, **14**, 9813.
6 H. Cheng, B. Huang, P. Wang, Z. Wang, Z. Lou, J. Wang, X. Qin, X. Zhang and Y. Dai, *Chem. Commun.*, 2011, **47**, 7054.
7 P. Wang, B. Huang, X. Zhang, X. Qin, H. Jin, Y. Dai, Z. Wang, J. Wei, J. Zhan, S. Wang, J. Wang and M. H. Whangbo, *Chem.–Eur. J.*, 2009, **15**(8), 1821.
8 J.-X. Sun, Y.-P. Yuan, L.-G. Qiu, X. Jiang, A.-J. Xie, Y.-H. Shen and J.-F. Zhu, *Dalton Trans.*, 2012, **41**, 6756.
9 Q. Li, Q. Yue, Q. H. Iwa, T. Kako and J. Ye, *J. Phys. Chem. C*, 2010, **114**, 4100.
10 R. S. Mane, W. J. Lee, H. M. Pathan and S.-H. Han, *J. Phys. Chem. B*, 2005, **109**, 24254.
11 W. Yao, B. Zhang, C. Huang, M. Chao, X. Song and Q. Xu, *J. Mater. Chem.*, 2012, **22**, 4050.
12 S. S. Yan, Z. S. Li and Z. G. Zo, *Langmuir*, 2009, **25**(17), 10397.
13 B. Yingpu, S. Ouyang, N. Umezawa, J. Cao and J. Ye, *J. Am. Chem. Soc.*, 2011, **133**, 6490.
14 C. T. Dinh, T. D. Nguyen, F. Kleitz and T. O. Do, *Chem. Commun.*, 2011, **47**, 7797.
15 X. Wang, K. Maeda, A. Thomas, K. Takanabe, G. Xin, J. M. Carlsson, K. Domen and M. Antonietti, *Nat. Mater.*, 2009, **8**, 76.
16 R. Asahi, T. Morikiwa, T. Ohwaki, K. Aoki and Y. Taga, *Science*, 2001, **293**, 269.
17 Y. Bi, S. Ouyang, J. Cao and J. Ye, *Phys. Chem. Chem. Phys.*, 2011, **13**, 10071.
18 Z. Yi, J. Ye, N. Kikugawa, T. Kako, S. Ouyang, H. S. Williams, H. Yang, J. Cao, W. Luo, Z. Li, Y. Liu and R. L. Withers, *Nat. Mater.*, 2010, **9**, 559.
19 A. Thomas, A. Fischer, F. Goettmann, M. Antonietti, J. O. Muller, R. Schlogl and J. M. Carlsson, *J. Mater. Chem.*, 2008, **18**, 4893.
20 J. M. Hu, *Appl. Phys. Lett.*, 2006, **89**, 261117.
21 K. Maeda, X. Wang, Y. Nishihara, D. Lu, M. Antonietti and K. Domen, *J. Phys. Chem. C*, 2009, **113**, 4940.
22 S. C. Yan, Z. S. Li and Z. G. Zou, *Langmuir*, 2010, **26**, 3894.
23 S. C. Yan, S. B. Lv, Z. S. Li and Z. G. Zou, *Dalton Trans.*, 2010, **39**, 1488.
24 Z. Ding, X. Chen, M. Antonietti and X. Wang, *ChemSusChem*, 2011, **4**, 274.
25 Y. Di, X. Wang, A. Thomas and M. Antonietti, *ChemCatChem*, 2010, **2**(7), 834.
26 C. Pan, J. Xu, Y. Wang, D. Li and Y. Zhu, *Adv. Funct. Mater.*, 2012, **22**(7), 1518.
27 Y. Wang, R. Shi, J. Lin and Y. Zhu, *Energy Environ. Sci.*, 2011, **4**, 2922.
28 S. C. Yan, Z. S. Li and Z. G. Zou, *Langmuir*, 2009, **25**(17), 10397.
29 N. Zhang, S. Q. Liu, X. Z. Fu and Y. J. Xu, *J. Phys. Chem. C*, 2011, **115**, 9136.
30 M. J. Bojdys, J. O. Muller, M. Antonietti and A. Thomas, *Chem.–Eur. J.*, 2008, **14**, 8177.
31 Y. Zhao, D. Yu, H. Zhou, Y. Tian and O. Yanagisawa, *J. Mater. Sci.*, 2005, **40**, 2645.
32 X. Li, J. Zhang, L. Shen, Y. Ma, W. Lei, Q. Cui and G. Zou, *Appl. Phys. A: Mater. Sci. Process.*, 2009, **94**, 387.
33 L. Ge, J. X. Jing, J. Wang, S. J. Wang, Q. Liu, F. Liu and M. J. Zhang, *J. Mater. Chem.*, 2011, **21**, 10750.
34 G. L. Huang and Y. F. Zhu, *J. Phys. Chem. C*, 2007, **111**, 11952.
35 M. Thomas, S. K. Ghosh and K. C. George, *Mater. Lett.*, 2002, **56**, 386.
36 N. Li, G. Liu, C. Zhen, F. Li, L. Zhang and H. M. Cheng, *Adv. Funct. Mater.*, 2011, **21**, 1717.
37 J. W. Tang, Z. G. Zou and J. H. Ye, *J. Phys. Chem. B*, 2003, **107**, 14265.
38 M. C. Long, W. M. Cai, J. Cai, B. X. Zhou, X. Y. Chai and Y. H. Wu, *J. Phys. Chem. B*, 2006, **110**, 20211.
39 J. S. Chen, Z. Y. Wang, X. C. Dong, P. Chen and X. W. Lou, *Nanoscale*, 2011, **3**, 2158.
40 H. Wang, Y. S. Bai, J. T. Yang, X. F. Lang, J. H. Li and L. Guo, *Chem.–Eur. J.*, 2012, **18**, 5524.
41 L. Xifeng, W. Qilong and C. Deliang, *J. Mater. Sci. Technol.*, 2010, **26**(10), 925.
42 N. Kakuta, N. Goto, H. Ohkita and T. Mizushima, *J. Phys. Chem. B*, 1999, **103**, 5917.
43 H. Tsutomu and V. K. Prashant, *Langmuir*, 2004, **20**(14), 5645.
44 S. C. Yan, S. B. Lv, Z. S. Li and Z. G. Zou, *Dalton Trans.*, 2010, **39**, 1488.

